JOURNAL OF GEOPHYSICAL RESEARCH, VOL. 98, NO. D6, PAGES 10,411–10,427, JUNE 20, 1993

Dimethylsulfide/Cloud Condensation Nuclei/Climate System: Relevant Size-Resolved Measurements of the Chemical and Physical Properties of Atmospheric Aerosol Particles

P. K. QUINN[1,2], D. S. COVERT [3,4], T. S. BATES[1,2,4], V .N. KAPUSTIN[5], D. C. RAMSEY-BELL[1,2], AND L. M. MCINNES[6]

Atmospheric aerosol particles resulting from the oxidation of dimethylsulfide (DMS) may have an impact on global climate if they result in an enhancement in the cloud condensation nuclei (CCN) number concentration and shortwave cloud albedo. To characterize and quantify relationships within the DMS/CCN/climate system, simultaneous measurements were made over the northeastern Pacific Ocean in April and May 1991 of particulate non-sea-salt sulfate, methanesulfonate, and ammonium mass size distributions, number size distributions of particles having diameters between 0.02 and 9.6 μm, CCN concentrations at 0.3% supersaturation, relative humidity, and temperature. Comparisons between particle mass and surface area indicate that non-sea-salt sulfate, methanesulfonate, and ammonium were not involved in new particle production on the 12- to 24-hour time scale of the measurements. Instead, high levels of available particulate surface area resulted in the condensation of the gas phase precursors onto existing aerosol. A doubling of non-sea-salt sulfate, methanesulfonate, and ammonium mass corresponded to a 40 to 50% increase in number in the accumulation mode size range. Likewise, a doubling of the non-sea-salt sulfate mass corresponded to a 40% increase in the CCN number concentration. As methanesulfonate made up a very small fraction of the soluble particulate mass, no correlations were found between methanesulfonate mass and CCN number. In a separate experiment, measurements were made of particulate non-sea-salt sulfate, methanesulfonate, and ammonium mass size distributions over the central Pacific Ocean during February 1991. The percent of methanesulfonate in the supermicrometer particle size fraction was greater in these samples than in those collected over coastal waters of the northeastern Pacific. In both regions the non-sea-salt sulfate mass size distributions were bimodal, while ammonium was found to be concentrated in larger accumulation mode particles.

1. INTRODUCTION

Twomey [1974, 1977] suggested that an increase in the cloud condensation nuclei (CCN) number population could affect global climate as it would result in an enhancement in cloud droplet concentration and shortwave cloud albedo. Recent satellite and aircraft measurements of ship tracks in stratus clouds [*Coakley et al.*, 1987; *Radke et al.*, 1989] offer experimental validation of this theory. The data show an increase in the reflectivity of thin marine stratus clouds in the region of ship tracks which corresponds to an increase in particle and cloud droplet concentrations and a decrease in droplet sizes. It also has been shown that in regions of low CCN concentrations an increase in the CCN number population corresponds to an increase in fractional cloudiness and, hence, global albedo [*Albrecht*, 1989].

The connection between CCN and cloud albedo has been extended to the natural atmosphere through the recognition of biogenic dimethylsulfide (DMS) as a potential source of CCN [*Nguyen et al.*, 1983; *Bigg et al.*, 1984; *Charlson et al.*, 1987]. DMS is formed in seawater through the enzymatic cleavage of dimethylsulfoniopropionate [*Cantoni and Anderson*, 1956; *Dacey and Blough*, 1987] which is produced by certain species of phytoplankton in the photic zone. It then is emitted to the atmosphere where it may be oxidized to gas phase dimethylsulfoxide (DMSO), dimethylsulfone ($DMSO_2$), SO_2, H_2SO_4, or methanesulfonic acid (MSA). The oxidation products can form new particles or contribute to the growth of existing particles through the processes of homogeneous and heterogeneous nucleation, respectively. As these species are water soluble, the resulting particles that have a large enough diameter act as CCN under appropriate atmospheric conditions.

Experimental evidence exists which indirectly confirms the role of DMS as a source of CCN. Sulfur isotope measurements of aerosol over the Pacific Ocean indicate that DMS can be the source of marine particulate non-sea-salt sulfate (nss $SO_4^=$) [*Calhoun et al.*, 1991]. Oceanic DMS emissions and condensation nuclei (CN) concentrations, when resolved by latitude and season, appear to be directly correlated [*Bates et al.*, 1987]. In regions where DMS fluxes are large, CN concentrations and incident solar radiation also are high. As CCN are a subset of CN, this suggests a link between changes in the DMS source strength and CCN concentration. Nine years of data from Cape Grim (41°S) show a seasonal correlation between CCN and MSA, a species derived solely from the oxidation of DMS, also indicating that DMS emissions influence CCN concentrations [*Ayers and Gras*, 1991]. A comparison of an index of aerosol particle size derived from

[1]National Oceanic and Atmospheric Administration, Pacific Marine Environmental Laboratory, Seattle, Washington.
[2]Also at The Joint Institute for the Study of the Atmosphere and Ocean, University of Washington, Seattle.
[3]Department of Environmental Health, University of Washington, Seattle.
[4]Also at Department of Atmospheric Sciences, University of Washington, Seattle.
[5]Institute of Atmospheric Physics, Russian Academy of Sciences, Moscow.
[6]Department of Chemistry, University of Washington, Seattle.

Paper number 93JD00467.
0148-0227/93/93JD-00467$05.00

satellite observations and seawater DMS concentrations from shipboard measurements reveal a correlation between the two parameters in the region of the tropical Pacific Ocean [*Durkee et al.*, 1991]. Satellite measurements also show a correlation between surface ocean chlorophyll concentrations and low-level cloud albedos over the central North Atlantic Ocean [*Falkowski et al.*, 1992] indicating that biogenic processes enhance the albedo of marine stratus.

Evidence of the sensitivity of the production of DMS to climate change has been seen in depth profiles of DMS oxidation products from the Vostok ice core. Over a complete glacial/interglacial cycle an increase in nss $SO_4^=$ and MSA concentrations has been observed during cold stages suggesting an enhancement in DMS production [*Legrand et al.*, 1991].

The relationship between an increase in DMS emissions, CCN concentrations, and cloud albedo is complicated by its dependence on many parameters. These include the source and sink processes controlling the burden of atmospheric DMS; DMS-derived particulate mass; CN in the nuclei, accumulation, and coarse modes; CCN; and cloud droplets. The long time constants for some of the multiphase transformation processes further complicates the relationship. The number of processes and multiple time constants involved has made it difficult to quantify the relationship between DMS and cloud albedo and, hence, to incorporate it into global climate models.

This paper will focus on relationships occurring within the atmospheric particulate phase between CN mass concentrations, CN number concentrations, and CCN number concentrations. These are the first reported simultaneous measurements of particulate phase mass size distributions of nss $SO_4^=$, MSA, and NH_4^+; number size distributions of particles having diameters between 0.02 and 9.6 μm; CCN concentrations at a supersaturation of 0.3%; relative humidity (RH); and temperature. The specific questions to be addressed include the following: (1) How are DMS oxidation products partitioned between the processes of new particle production and particle growth; what fraction leads to the production of fresh nuclei mode particles; what fraction allows for the growth of particles to CCN size; and what fraction condenses onto particles already large enough to act as CCN? (2) How does this partitioning vary from open ocean to coastal regions? (3) What role does atmospheric gas phase NH_3 play in new particle production and particle growth? (4) Can relationships between particle number and mass and CCN number be quantified based on observations in the marine boundary layer?

2. STUDY AREA AND METEOROLOGY

The measurements were made during two field experiments. The first was on board the NOAA ship *Discoverer* during a cruise whose purpose was to study radiatively important trace species (RITS). The ship traveled from Seattle, Washington to Hilo, Hawaii during February 1991. The second was during the Pacific sulfur/stratus investigation (PSI) which took place in April and May 1991. Samples were collected simultaneously at the University of Washington research station at Cheeka Peak and aboard the NOAA ship *Discoverer*. Cheeka Peak is a mountaintop site (480 m) located 2 km from the Washington coast at 48°18'N and 124°37'W. The shipboard measurements were made from 0 to 300 km offshore at the same latitude as Cheeka Peak. Hence the two experiments provided the opportunity to obtain measurements from an open ocean region, a coastal ocean region, and a midboundary layer land-based site.

During RITS 91, samples were collected as time permitted and without regard to changes in local conditions such as true wind direction and relative humidity. The sampling period, average latitude and longitude, relative humidity, and surface wind direction for each sample are listed in Table 1. Radiosonde measurements and trajectory calculations were not available for this cruise.

During PSI 91, sampes were collected over time periods in which the local wind direction, relative humidity, and CN count remained fairly constant. The time period of sampling, average latitude and longitude for the shipboard samples, height of the mixed layer (defined as the height of the top of the lowest cloud layer), average relative humidity and surface wind direction, and trajectory classification of the sampled air mass are given in Table 1.

In the following discussion, both the PSI 91 ship and Cheeka Peak samples are divided into two groups. The first includes those samples collected between Julian days 106.99 and 115.44 (local) when, according to the air mass trajectories, the sampled air had originated at the surface, was mixed into the free troposphere, then subsided from aloft and passed over Canada in the 2 or 3 days prior to sampling. The vertical mixing resulted in an air mass influenced by both marine and continental sources. The second group includes samples collected between Julian days 115.5 and 119.18 (local). The air mass trajectories showed no evidence of subsidence and that the air had come from a northwesterly to westerly direction passing over the ocean surface for several days prior to being sampled. A trajectory from each period is shown in Figure 1.

3. MEASUREMENTS

The measurements made during RITS 91 and during PSI 91 on board the ship and at Cheeka Peak are listed in Table 2. During RITS 91, samples were collected for the determination of the mass size distributions of nss $SO_4^=$, MSA, Na^+, and NH_4^+. Contamination by the ship was avoided by collecting samples only when the CN count was less than 1000 cm^{-3} for particles having diameters greater than 0.015 μm, the wind speed was greater than 3 m s^{-1}, and the wind direction was forward of the ship's beam.

During PSI 91, samples were collected continuously for the measurement of particle number size distributions. Shipboard measurements covered the size range of 0.02 to 0.6 μm in particle diameter and Cheeka Peak measurements encompassed the size range of 0.02 to 9.6 μm. Samples were collected for the determination of the mass size distributions of nss $SO_4^=$, MSA, Na^+, and NH_4^+ over time periods in which the local atmospheric conditions remained fairly constant. Contamination of samples by local sources was prevented by sampling only during periods of local surface westerly flow, when the CN count was less than 1000 cm^{-3} for particles having a diameter greater than 0.015 μm, and when the wind speed was greater than 3 m s^{-1}. In addition, shipboard samples were collected only when the relative wind direction was forward of the ship's beam.

A seven-stage cascade impactor [*Berner et al.*, 1979] was used to collect samples for the determination of mass size distributions of nss $SO_4^=$, MSA, Na^+, and NH_4^+. The stages had upper size cuts of 0.16, 0.25, 0.5, 1.0, 2.0, and 4.0 μm in particle diameter. The stage with a nominal upper size cut of 8.0 μm was discarded. Tedlar films were used as the collection substrate for the five largest stages and a Millipore Fluoropore filter (1.0-μm pore size) was used for the smallest stage. The

TABLE 1. Sampling Times, Positions, Mixed Layer Height, Percent RH, Surface Wind Direction, and Trajectory for RITS 91 and PSI 91 Samples

Sample	Start-Stop Times, LT	Position	Height of Mixed Layer, m	RH, %	Surface Wind Direction	Trajectory
			RITS 91			
1	52.979–53.921	40.46°N 135.00° W		83 ± 7.6	110 ± 20	
2	54.021–55.804	35.74°N 136.5°W		76 ± 12	106 ± 17	
3	55.875–56.667	30.89°N 140.6°W		86 ± 11	204 ± 62	
4	56.938–58.554	27.19°N 146.4°W		76 ± 8.4	259 ± 28	
5	58.833 59.833	22.75°N 152.1°W		76 ± 5	288 ± 17	
			PSI 91, Ship			
1	106.99–108.42	48.2°N 128.4°W	500 ± 57	78 ± 4	326 ± 8.8	from Canada/ subsidence
2	108.47–109.67	48.3°N 128.4°W	475 ± 25	79 ± 4	329 ± 9	from Canada/ subsidence
3	109.71–111.32	48.4°N 128.4°W	450 ± 120	87 ± 2	335 ± 13	from Canada/ subsidence
4	111.87–112.66	48.2°N 125.4°W	1070 ± 210	70 ± 8	277 ± 30	from Canada/ subsidence
5	113.97–115.44	48.2°N 126.3°W	mixed through FT	65 ± 5	242 ± 32	from Canada and west / subsidence
6	115.48–116.74	48.3°N 128.2°W	1300 ± 103	70 ± 6	226 ± 50	from NW/no subsidence
7	117.34–118.22	48.0°N 125.1°W	1380	63 ± 5	227 ± 65	from NW/no subsidence
8	119.47–120.67	48.2° N 127.9°W	450 ± 40	76 ± 6	174 ± 84	from west/no subsidence
			PSI 91, Cheeka Peak			
1	107.59–108.25		500 ± 57	81 ± 16	245 ± 7.3	from Canada/ subsidence
2	108.85–109.00		475 ± 25	99 ± 12	279 ± 7.6	from Canada/ subsidence
3	111.83–112.88		1070 ± 210	95 ± 42	261 ± 28	from Canada/ subsidence
4	113.38–115.27		mixed through FT	94 ± 73	233 ± 31	from Canada and west/ subsidence
5	115.35–116.10		1300 ± 103	84 ± 74	246 ± 54	from NW/no subsidence
6	116.75–118.11		1380	89 ± 54	260 ± 74	from NW/no subsidence
7	118.58–119.18		930 ± 630	85 ± 38	272 ± 78	from west/no subsidence

The mixed layer height is defined as the height of the top of the lowest cloud layer. FT, free troposphere. RH, relative humidity. RITS, radiatively important trace species. PSI, Pacific sulfur/stratus investigation.

Millipore filter has a 99% collection efficiency for particles with diameters larger than 0.035 μm [*Liu and Lee*, 1976]. An impaction stage ($D_p \cong 10$ μm) at the inlet of the impactor was covered with silicone grease to prevent bouncing of large particles onto the downstream stages.

Prior to use, films were sonicated in 10% H_2O_2 for 30 min, rinsed 6 times in distilled, deionized water, and dried in an NH_3 and SO_2 free glove box. All handling of the substrates was done in the glove box. Blank levels were determined by loading the impactor with the substrates and deploying it at the sampling site for the length of a typical sampling period without pulling air through it. Following collection, the blanks were treated in an identical manner as the sample substrates. On average, the Na^+ and $SO_4^=$ blanks were 9 and 1% of the sample values, respectively. The MSA and NH_4^+ blanks were below detection limit.

The time period of sampling ranged from 12 to 24 hours. After sample collection the material on the films and filter was extracted by first wetting with 1 ml of methanol, then adding 5 ml of distilled deionized water, and sonicating for 15 min. Extracts were analyzed by ion chromatography for Na^+, NH_4^+, $SO_4^=$, and MSA. The cation analysis was performed with a Dionex CS-1 column, 0.5-mM HCl eluent, and 68-mM tetramethylammonium hydroxide monohydrate regenerant.

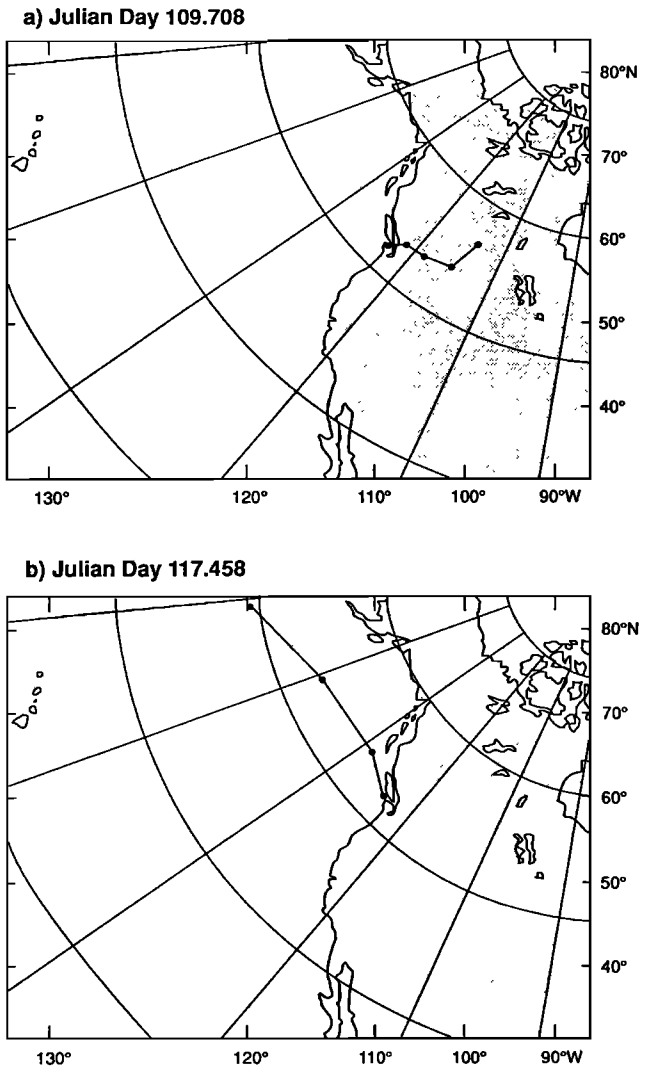

Fig. 1. Trajectory analyses calculated by a medium-range forecast (MRF) model for (*a*) Julian day 109.708 (local) and (*b*) Julian day 117.458 (local). The trajectories are initiated at a fixed height above the ocean surface and are allowed to move vertically using the MRF vertical wind fields. Each circle signifies one day back in time.

Sulfate ($SO_4^=$) analysis was done with a Dionex AS-4A column, 0.75-mM $NaHCO_3$/2.0-mM Na_2CO_3 eluent, and 12.6-mM H_2SO_4 regenerant. MSA analysis was performed with a Dionex AS-4 column, a 5-mM NaOH mobile phase to elute the weak organic acids followed by 100-mM NaOH to elute the stronger acids, and 12.6-mM H_2SO_4 regenerant. Non-sea-salt $SO_4^=$ concentrations were calculated from Na^+ concentrations and the molar ratio of sulfate to sodium in seawater of 0.0603. All particulate chemical concentrations are reported in nmol m^{-3} at 25°C and 1 atm.

One-minute averages of the number concentration of particles greater than 0.015 μm were measured with a particle counter (TSI model 3760, St. Paul, Minnesota). A Permapure diffusion drier was placed upstream to lower the relative humidity of the sample stream to near 25%.

The number size distribution of particles having diameters between 0.02 and 0.6 μm was measured with a differential mobility analyzer (DMA) (TSI model 3071; *Liu and Pui* [1975]). A krypton 85 charge neutralizer (TSI model 3077) was put upstream to produce an equilibrium charge distribution. Also upstream was a diffusion drier to reduce the relative humidity of the sample air to less than 25% and an impactor with a 50% cutoff diameter of 0.7 μm to bound the upper limit of the inversion algorithm.

Narrow electrical mobility increments of the particle distribution were selected over a sequence of 17 steps in a time period of 15 min or less. The number concentration in each increment was measured with a particle counter (TSI model 3760) at a flow rate of 1 l min^{-1}. A minimum of 1000 particles was counted in each size increment yielding an uncertainty of about 3% for one standard deviation and the assumption of Poisson counting statistics. The number concentration was corrected for the counting efficiency of the particle counter [*Zang and Liu*, 1991] and diffusion losses in the DMA [*Reineking and Porstendorfer*, 1986]. A Boltzmann-Fuchs equilibrium charge distribution was assumed to be present on the particles analyzed. The number mobility distribution was inverted to a number size distribution using an algorithm similar to that provided by the manufacturer [*Keady et al.*, 1983].

The size distribution of those particles with diameters between 0.6 and 9.6 μm was measured with an aerodynamic particle sizer (APS) (TSI model 3300; *Baron* [1986]). A Permapure diffusion drier was placed upstream of the APS to reduce the relative humidity of the sample stream to near 25% at the instrumental temperature. The sheath air was cleaned with filters and charcoal and was at a humidity less than 20%. The sample and sheath airflow rates used were those at which the APS was calibrated by the manufacturer. All flow rates were checked in the field and adjusted to better than 1%.

The DMA and APS data were edited to eliminate outlying points resulting from local contamination or instrument disruption. Any scans in which concentrations at adjacent diameters differed by more than a factor of 2 were discarded. To compare the number and mass size distributions, the DMA

TABLE 2. Measurements Made During RITS 91 and PSI 91 Aboard the Ship and at Cheeka Peak

	RITS 91	PSI 91 Ship	PSI 91 Cheeka Peak
Mass size distributions of nss $SO_4^=$, MSA, and NH_4^+	•	•	•
Total number concentration of particles with $D_p > 0.15$ μm	•	•	•
Number size distribution of particles with $0.02 < D_p < 0.6$ μm		•	
Number size distribution of particles with $0.02 < D_p < 9.6$ μm			•
CCN concentration at 0.3% supersaturation			•
Surface temperature and dew point	•	•	•
Surface wind speed and direction	•	•	•
Temperature and dew point aloft		•	•
Calculated air mass trajectories		•	•

MSA, methanesulfonic acid; CCN, cloud condensation nuclei; nss, non-sea-salt sulfate. Circle indicates that the parameter was measured.

and APS data were averaged over the actual impactor sampling time periods.

On board the ship, sample air for the determination of number size distributions was drawn through a 15-m inlet line. The top of the inlet was about 25 m above the ocean surface and 10 m forward of the ship's stack. The air was dried to a relative humidity near 25% by heating prior to sample collection. The impactor was located outside approximately 15 m above the ocean surface and 10 m forward of the ship's stack and, hence, collected air at ambient RH. At Cheeka Peak, air for the determination of both number and mass size distributions was drawn from a height of 10 m and heated such that the RH was about 25%. To compare size distributions measured from wet and dry air, those collected dry were corrected for the effect of relative humidity on particle diameter. Corrections for particle diameters less than 1.0 μm were made using the measured local RH, a reference RH of 25% representing the dried sample stream, the measured NH_4^+ to nss $SO_4^=$ molar ratio, and sulfate growth curves [*Charlson et al.*, 1978]. Corrections for diameters larger than 1.0 μm were made using the measured RH and NaCl growth curves [*Tang et al.*, 1977].

CCN concentrations were measured with a static thermal diffusion cloud chamber at 0.3% supersaturation. At this supersaturation all particles with diameters greater than 0.073 μm will activate assuming a composition of pure $(NH_4)_2SO_4$ [*Fletcher*, 1962]. The sampled air was drawn from the same flow as that used for the DMA and APS measurements.

Ancillary measurements included surface temperature, dew point, wind speed, and wind direction. Temperature and dew point aloft were measured at least twice per day with radiosondes [*Johnson and Mitchell*, 1991]. Air mass back trajectories were calculated using the hybrid single-particle Lagrangian integrated trajectories (HY-SPLIT) model based on wind fields generated by the medium-range forecast (MRF) model [*Draxler*, 1992]. The trajectories were calculated such that they started at a fixed height of 480 m above the ocean surface and were allowed to move horizontally and vertically using the MRF vertical wind fields.

4. Results and Discussion

4.1. *Number Size Distributions*

During PSI 91, number size distributions were measured for particle diameters from 0.02 to 0.6 μm on board the ship and from 0.02 to 9.6 μm at Cheeka Peak. The distributions were determined from measurements of a dried sample stream and were corrected for RH effects on particle diameter. Shown in Figure 2 are the distributions that represent the aerosol under local humidity conditions. The geometric mean diameter (D_{gn}), geometric standard deviation (σ_g), and total number (N) for each submicron mode of the average number size distributions are listed in Table 3. The distributions were bimodal in the submicron range at both locations. On board the ship, when air was coming from aloft and over Canada, the average and standard deviation of the nuclei and accumulation mode concentrations were 200 ± 109 and 140 ± 53 cm^{-3}, respectively. When air was coming from the west, the average nuclei and accumulation concentrations were 460 ± 150 and 130 ± 43 cm^{-3}, respectively. At Cheeka Peak, when air was coming from the north, the average nuclei and accumulation mode concentrations were 320 ± 110 and 99 ± 36 cm^{-3}, respectively. During westerly flow the average nuclei and accumulation mode concentrations were 330 ± 120 and 76 ± 27 cm^{-3}, respectively.

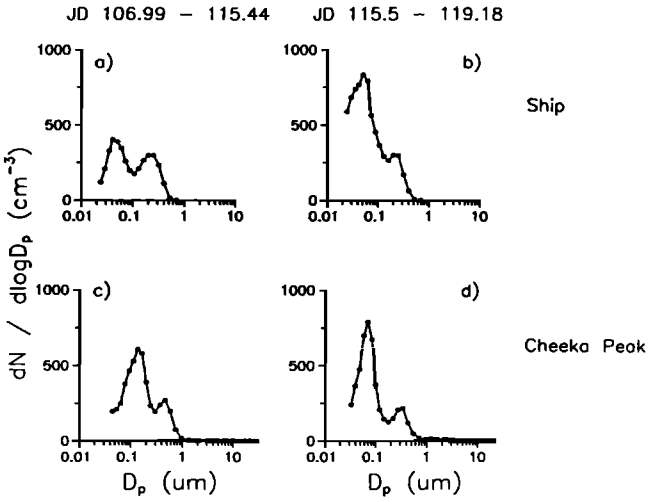

Fig. 2. Particle number size distributions measured during the Pacific sulfur/stratus investigation (PSI 91). Distributions were corrected for relative humidity effects on particle diameters and were averaged over the time period of the corresponding impactor sample. Average distribution corresponding to (*a*) shipboard impactor samples 1, 2, 3, 4, and 5 as air was arriving from aloft and over Canada; (*b*) shipboard impactor samples 6, 7, and 8 during westerly airflow; (*c*) Cheeka Peak impactor samples 1, 2, 3, and 4 as air was arriving from aloft and over Canada; and (*d*) Cheeka Peak impactor samples 5, 6, and 7 during westerly airflow.

For all samples collected on board the ship, an average of 41% of the submicron particles were in the nuclei mode. At Cheeka Peak, 80% were contained in this mode. The minimum between the nuclei and the accumulation modes occurred at 0.12 ± 0.02 μm in the shipboard distributions and at 0.22 ± 0.08 μm at Cheeka Peak. The higher concentration of nuclei relative to accumulation mode particles at Cheeka Peak resulted in a shift of the intermode minimum to a larger diameter. The concentration of supermicron particles averaged over all samples at Cheeka Peak was 2.7 ± 2.6 cm^{-3}.

4.2. *Comparison of Mass and Surface Area Size Distributions*

The particulate mass derived from the homogeneous and heterogeneous nucleation of gas phase H_2SO_4 and MSA will increase the CCN number concentration if the resulting particles grow to a size large enough to nucleate cloud droplets at the 0.3 to 0.6% supersaturations of stratus and stratocumulus clouds. However, if H_2SO_4 and MSA condense onto existing particles already large enough to act as CCN, their only effect on the CCN number population will be to increase the water solubility of the particles if they were composed primarily of organic or crustal material and decrease the supersaturation at which activation will occur.

The distribution of gaseous species between the processes of new particle production and particle growth is a function of the saturation vapor pressure of the condensing species, the ambient water vapor pressure, temperature, and characteristics of the existing aerosol. The latter includes the chemical properties of *p*H and presence of surface films as well as the physical properties of number and surface area size distributions. The reaction of NH_3 with acidic aerosol can enhance condensation onto existing particles by increasing the

TABLE 3. D_{gn}, σ_g, and N for Each Submicron Mode of the Average Number Size Distributions Measured During PSI 91 Aboard the Ship and at Cheeka Peak

	D_{gn}, μm		σ_g, μm		N, cm^{-3}	
Trajectory	$D_p < 0.1$	$D_p < 0.6$	$D_p < 0.1$	$D_p < 0.6$	$D_p < 0.1$	$D_p < 0.6$
			Ship			
from Canada/ subsidence	0.040	0.25	1.6	1.8	200 ± 109	140 ± 53
from NW/no subsidence	0.045	0.25	1.6	1.8	460 ± 150	130 ± 43
	$D_p < 0.2$	$D_p < 1.0$	$D_p < 0.2$	$D_p < 1.0$	$D_p < 0.2$	$D_p < 1.0$
			Cheeka Peak			
from Canada/ subsidence	0.15	0.45	1.6	1.7	320 ± 110	99 ± 36
from NW/no subsidence	0.06	0.35	1.5	1.8	330 ± 120	76 ± 27

Particle diameters, D_p, were corrected for effects of RH on particle size using the measured ambient RH, a reference RH of 25% representing the dried sample stream, the measured NH_4^+ to nss $SO_4^=$ molar ratio, and sulfate growth curves [*Charlson et al.*, 1978].

*p*H of the particle and lowering the surface acid vapor pressure [*Hoppel*, 1987; *Quinn et al.*, 1992]. Alternatively, the presence of particulate surface films may inhibit condensation of gaseous species. Existing particles can provide a sink for gaseous species, thereby suppressing new particle production [*Warren and Seinfeld*, 1985; *Covert et al.*, 1992].

Results from laboratory studies indicate that for the H_2SO_4/MSA/H_2O system, nucleation of new particles results primarily from the formation of stable H_2SO_4 and H_2O clusters, while growth occurs by condensation of H_2SO_4, MSA, and H_2O [*Hoppel*, 1987; *Hoppel et al.*, 1987; *Kreidenweis et al.*, 1991]. The greater nucleating potential of H_2SO_4 is a result of the lower acid vapor concentration required for nucleation with water vapor; it is about 2 orders of magnitude less than for the nucleation of MSA with H_2O [*Hoppel*, 1987].

If the condensation of a gaseous species with water vapor and/or other gas phase compounds results in new particle production, that species should be present initially in particles with diameters less than 0.01 μm. If the condensation of a species onto preexisting particles results in particle growth, it should be distributed across the particle size range as a function of particulate effective surface area. The effective surface area depends on both the available particle surface area and the physical process of the collision of the gas molecule with the particle as a function of particle size. The presence of clouds may confuse the relationship between mass and effective surface area, however. Cycling through clouds contributes to the bimodality of the submicron portion of the number size distribution [*Hoppel et al.*, 1987]. Alternatively, a proximity to clouds may enhance new particle production but not particle growth [*Raes and Van Dingenen*, 1992]. With a high concentration of new particles the available H_2SO_4 is spread over more particles so that these smaller particles grow to CCN size over very long time scales. Depending on the concentration and size distribution of sea-salt particles, it may offset this effect and increase CCN production by enhancing the heterogeneous oxidation of SO_2 to sulfate [*Hegg et al.*, 1992]. In any case, a comparison between mass and effective surface area size distributions is a useful starting point in determining how a gaseous species has been partitioned between the processes of particle production and growth.

4.2.1. *Mass size distributions.* Mass size distributions of nss $SO_4^=$, MSA, and NH_4^+ were measured during RITS 91 and PSI 91. The mass concentrations for Na^+, nss $SO_4^=$, MSA, and NH_4^+ as a function of size for each sample collected are given in Table 4. The nss $SO_4^=$ size distributions are shown in Figure 3. During RITS 91, 60% of the measured nss $SO_4^=$ size distributions were bimodal with 12 ± 9% of the nss $SO_4^=$ occurring in supermicron particles. During PSI 91, as air was coming from aloft and over Canada, 80% of the size distributions on the ship and 25% at Cheeka Peak were bimodal with 11 ± 8 and 11 ± 6% of the nss $SO_4^=$ occurring in the supermicron fraction, respectively. During onshore flow, all measured nss $SO_4^=$ size distributions were bimodal. On the ship and at Cheeka Peak, 24 ± 20 and 25 ± 10% of the nss $SO_4^=$ mass was present in the supermicron fraction, respectively.

The maximum in the submicron portion of the size distribution occurred between 0.16- and 0.25-μm diameter during RITS 91. Measurements during PSI 91 show the submicron maximum to occur between 0.25 and 0.5 μm on board the ship and between 0.37 and 0.75 μm at Cheeka Peak. The supermicron maximum occurred between 1 and 3 μm during RITS 91 and on board the ship during PSI 91. At Cheeka Peak, however, the supermicron maximum occurred over a broader range of 1 to 9.6 μm. Higher humidities at Cheeka Peak (see Table 1) led to a shift toward larger particle sizes in the number size distribution and in the submicron and supermicron maximum of the mass size distributions. The higher humidities also may have led to the broadening of the

TABLE 4. Mass Concentrations of Na^+, nss $SO_4^=$, MSA, and NH_4^+ as a Function of Size for Each Impactor Sample Collected During RITS 91 and PSI 91

Sample	Stage	D_{gn}, μm	Concentrations, nmol m^{-3} μm^{-1}			
			$Na^+/d \log D_p$	nss $SO_4^=/d \log D_p$	MSA/$d \log D_p$	$NH_4^+/d \log D_p$
			RITS 91			
1	1	0.113	19.00	<.02	0.04	<.02
	2	0.200	10.00	4.20	0.29	2.10
	3	0.353	<.02	5.80	0.22	3.00
	4	0.707	2.90	1.90	0.10	<.02
	5	1.410	13.00	1.40	0.09	<.02
	6	2.830	49.00	2.60	0.12	<.02
2	1	0.113	109.00	<.02	—	<.02
	2	0.200	9.05	8.40	—	<.02
	3	0.353	6.40	7.02	—	<.02
	4	0.707	7.40	2.03	—	<.02
	5	1.410	19.00	1.80	—	<.02
	6	2.830	74.00	2.90	—	<.02
3	1	0.113	0.43	8.10	0.01	<.02
	2	0.200	0.11	12.00	0.32	16.00
	3	0.353	1.40	8.20	0.25	9.00
	4	0.707	19.00	0.90	0.02	<.02
	5	1.410	90.00	0.56	0.08	<.02
	6	2.830	150.00	0.11	0.03	<.02
4	1	0.113	2.00	0.25	<.008	<.02
	2	0.200	8.80	3.20	0.06	<.02
	3	0.353	18.00	1.50	0.03	<.02
	4	0.707	47.00	<.02	0.02	<.02
	5	1.410	130.00	<.02	0.08	<.02
	6	2.830	270.00	0.35	0.06	<.02
5	1	0.113	2.00	0.38	<.008	<.02
	2	0.200	0.59	9.50	0.05	3.70
	3	0.353	3.90	7.50	0.09	3.10
	4	0.707	14.00	2.10	0.04	0.15
	5	1.410	67.00	1.60	0.14	0.29
	6	2.830	140.00	0.45	0.10	<.02
			PSI 91, Ship			
1	1	0.128	0.47	0.36	0.01	<.02
	2	0.247	<.02	7.30	0.16	5.40
	3	0.446	0.79	25.00	0.36	14.00
	4	0.707	4.10	0.99	0.14	8.00
	5	1.414	27.00	2.40	0.04	<.02
	6	2.828	82.00	2.01	0.05	<.02
2	1	0.129	<.02	0.35	0.03	<.02
	2	0.238	<.02	6.10	0.17	3.80
	3	0.422	0.05	11.00	0.24	5.70
	4	0.707	2.20	5.04	0.08	2.60
	5	1.414	20.10	1.07	0.03	<.02
	6	2.828	62.00	0.63	0.01	<.02
3	1	0.135	0.47	0.39	0.03	<.02
	2	0.265	<.02	3.90	0.24	2.40
	3	0.457	0.65	14.00	1.57	6.40
	4	0.707	4.40	13.00	1.37	5.20
	5	1.414	25.00	2.60	0.22	0.68
	6	2.828	85.00	1.50	0.14	0.73
4	1	0.122	0.39	0.12	0.02	0.87
	2	0.230	0.10	10.10	0.41	7.10
	3	0.389	8.80	23.00	1.44	12.00
	4	0.707	2.02	6.30	0.47	3.20
	5	1.414	5.04	1.90	0.53	<.02
	6	2.828	12.00	1.70	0.10	<.02

TABLE 4. (continued)

Sample	Stage	D_{gn}, μm	Concentrations, nmol m^{-3} μm^{-1}			
			$Na^+/d \log D_p$	nss $SO_4^{=}/d \log D_p$	MSA/$d \log D_p$	$NH_4^+/d \log D_p$
			PSI 91, Ship			
5	1	0.120	0.52	0.27	0.03	<.02
	2	0.235	0.31	4.80	0.20	3.60
	3	0.393	0.90	6.10	0.17	4.90
	4	0.707	6.80	1.20	0.05	0.71
	5	1.414	11.00	1.00	0.18	<.02
	6	2.828	31.00	2.20	0.09	<.02
6	1	0.122	0.90	0.22	0.03	<.02
	2	0.243	2.20	2.90	0.14	2.90
	3	0.406	3.40	5.60	0.27	4.20
	4	0.707	19.00	1.20	0.10	0.48
	5	1.414	31.00	2.40	0.35	<.02
	6	2.828	68.00	3.10	0.17	<.02
7	1	0.113	0.33	0.26	0.04	0.76
	2	0.236	2.20	3.20	0.20	6.20
	3	0.395	1.70	6.90	0.25	3.90
	4	0.707	3.20	2.20	0.14	12.00
	5	1.414	33.00	3.20	0.39	<.02
	6	2.828	81.00	5.90	0.26	<.02
8	1	0.104	0.18	1.10	0.18	1.10
	2	0.202	13.00	11.00	0.59	9.50
	3	0.359	4.00	21.00	0.79	16.00
	4	0.707	17.00	8.40	0.40	5.60
	5	1.414	85.00	<.02	0.42	0.38
	6	2.828	200.00	4.20	0.37	<.02
			PSI 91, Cheeka Peak			
1	1	0.170	1.05	4.80	<.008	<.02
	2	0.300	3.80	9.20	0.55	11.00
	3	0.530	3.20	8.50	0.34	8.60
	4	1.061	3.70	1.70	0.04	<.02
	5	2.168	7.10	1.50	0.02	7.90
	6	5.373	6.10	1.10	0.01	<.02
2	1	0.339	8.20	3.60	0.26	<.02
	2	0.600	19.00	13.00	0.84	14.00
	3	1.059	12.00	8.30	0.41	8.60
	4	2.121	10.20	2.20	<.008	8.50
	5	5.477	9.80	1.30	0.10	4.60
	6	13.574	7.10	1.20	<.008	<.02
3	1	0.249	1.10	3.30	0.18	<.02
	2	0.440	3.00	7.20	0.66	8.00
	3	0.777	2.20	6.80	0.31	7.00
	4	1.556	1.90	1.10	0.05	<.02
	5	2.967	6.30	0.80	0.02	<.02
	6	7.353	9.30	0.84	0.03	<.02
4	1	0.249	2.10	2.20	0.09	<.02
	2	0.440	2.60	4.70	0.13	4.80
	3	0.777	3.60	2.10	0.04	<.02
	4	1.556	5.50	0.67	0.03	<.02
	5	2.967	16.00	0.52	<.008	<.02
	6	7.353	17.00	0.81	0.02	<.02
5	1	0.181	3.80	3.00	0.28	<.02
	2	0.320	7.00	9.50	0.75	9.30
	3	0.565	5.20	3.40	0.18	<.02
	4	1.131	6.80	0.70	0.14	<.02
	5	2.396	28.00	1.30	0.08	<.02
	6	5.939	19.00	0.93	0.01	<.02

TABLE 4. (continued)

Sample	Stage	D_{gn}, μm	Concentrations, nmol m^{-3} μm^{-1} $Na^+/d \log D_p$	nss $SO_4^{=}/d \log D_p$	MSA/$d \log D_p$	$NH_4^+/d \log D_p$
			PSI 91, Cheeka Peak			
6	1	0.192	3.20	3.30	0.13	0.88
	2	0.340	3.30	6.60	0.58	6.50
	3	0.600	4.60	4.20	0.22	1.70
	4	1.202	12.00	1.60	0.20	<.02
	5	2.510	47.00	3.50	0.26	<.02
	6	6.222	49.00	2.60	0.11	<.02
7	1	0.181	3.70	3.40	0.19	<.02
	2	0.320	4.20	5.80	0.20	2.80
	3	0.565	4.80	3.00	0.15	<.02
	4	1.131	19.00	2.30	0.14	<.02
	5	2.396	52.00	2.60	0.12	<.02
	6	5.939	28.00	2.50	0.04	<.02

Concentrations are given as nmol m^{-3} μm^{-1} representing the mass concentration per unit increment of size of each stage. The value of $d \log D_p$ for stages 1 = 0.301, 2 = 0.194, 3 = 0.301, 4 = 0.301, 5 = 0.301, and 6 = 0.301. The geometric mean diameter, D_{gn}, for the RITS 91 samples was based on the lower and upper size limits of the impactor stage. D_{gn} for the PSI 91 samples was derived from the measured number size distributions.

nss $SO_4^{=}$ mass distribution in the supermicron fraction.

Samples collected in the open ocean versus coastal regions did not vary greatly in the degree of partitioning of nss $SO_4^{=}$ between the submicron and the supermicron modes. However, these results indicate a larger amount of nss $SO_4^{=}$ mass occurring in the supermicron size range than noted in previously reported data derived from impactor measurements. These earlier measurements were made in both coastal and open ocean regions [*Savoie and Prospero*, 1982; *Saltzman et al.*, 1983, 1986; *Pszenny et al.*, 1989; *Pszenny*, 1992; *Huebert et al.*, 1993]. The only measurement indicative of a bimodal distribution was from the coastal region of the Antarctic [*Pszenny et al.*, 1989]. However, measurements made with Nuclepore and Teflon filters in series over the Northeast Pacific Ocean [*Andreae et al.*, 1988], the Antarctic [*Berresheim*, 1987], and southern Australia [*Berresheim et al.*, 1990] have shown up to 50% of the nss $SO_4^{=}$ in the supermicron fraction. This large fraction of coarse mode nss $SO_4^{=}$ could be a result of the condensation of SO_2 in addition to H_2SO_4 onto the sea-salt coated Nuclepore filters or a wide cut in the size segregation [*Quinn and Bates*, 1989].

All MSA size distributions (Figure 4) measured during RITS 91 were bimodal with 41 ± 18% of the mass in the supermicron fraction. During northerly winds from Canada, 60% of the shipboard and 75% of the Cheeka Peak samples from PSI 91 were bimodal. The fraction of MSA on supermicron particles was 17 ± 10 and 5.9 ± 4.8% on board the ship and at Cheeka Peak, respectively. During westerly flow, all of the shipboard and 67% of the Cheeka Peak samples were bimodal with 41 ± 24 and 19 ± 15% of the MSA mass present in the large particles, respectively.

The submicron maximum occurred in the diameter range of 0.16 to 0.25 μm for the RITS 91 samples and in the 0.25- to 0.5-μm range for the PSI 91 shipboard and Cheeka Peak samples. The supermicron maximum occurred between 1.0 and 2.0 μm for the RITS 91 and shipboard PSI 91 samples and over a broader range of 1.9 to 9.6 μm for the Cheeka Peak samples. Again, the higher humidities measured at Cheeka Peak may explain the difference in the position of the peaks and the shape of the supermicron portion of the mass size distributions.

The occurrence of a higher percent of supermicron MSA in the open ocean samples agrees with previously reported data. MSA size distributions from the Gulf of Mexico, Miami, the Peruvian coast, and the Antarctic coast did not have a peak in the supermicron fraction [*Saltzman et al.*, 1983, 1986; *Pszenny et al.*, 1989], while those measured over the tropical Pacific Ocean did [*Pszenny*, 1992; *Huebert et al.*, 1993]. The difference could be a result of a higher relative number concentration of supermicron particles over the open ocean and, hence, a larger amount of available surface in this size range. However, without measurements of the number size distribution it is difficult to say.

At all locations studied, the MSA to nss $SO_4^{=}$ molar ratio varied with respect to particle size. During RITS 91, the ratio ranged from <1 to 30% over all sizes with the largest ratios occurring in supermicron particles. During PSI 91 the shipboard molar ratio varied from <1 to 90% and the Cheeka Peak ratio from <1 to 21% over all impactor stages. Chemical and physical processes which produce and transform aerosol particles are size dependent as are particle optical properties and lifetimes. As a result, using a bulk-derived value for a parameter that varies with size, such as the MSA to nss $SO_4^{=}$ molar ratio, can obscure useful information and lead to inaccurate data interpretation.

No NH_4^+ was found in supermicron particles in the RITS 91 or shipboard PSI 91 samples and was detected in the supermicron fraction in only two of seven Cheeka Peak PSI 91 samples (Figure 5). Ammonium (NH_4^+) was detected in the smallest size range in only three samples from all experiments combined. The maximum in the size distribution was between

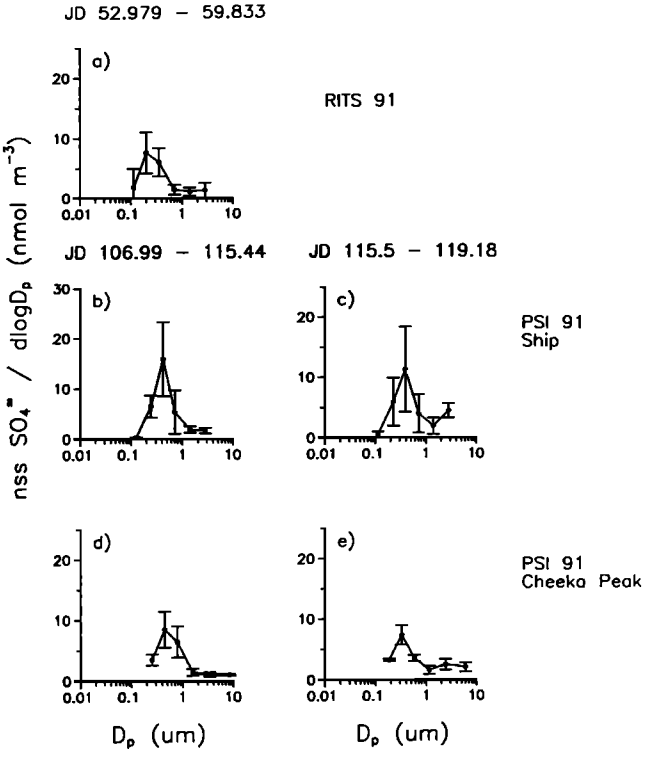

Fig. 3. Mass size distributions of non-sea-salt (nss) $SO_4^=$ from measurements during the radiatively important trace species cruise (RITS 91) and shipboard and Cheeka Peak measurements during PSI 91. Cheeka Peak distributions were based on measurements of dried air and were corrected for relative humidity effects on particle diameters. Average distribution of (*a*) impactor samples 1, 2, 3, 4, and 5 during RITS 91; (*b*) shipboard impactor samples 1, 2, 3, 4, and 5 as air was arriving from aloft and over Canada; (*c*) shipboard impactor samples 6, 7, and 8 during westerly airflow; (*d*) Cheeka Peak impactor samples 1, 2, 3, and 4 as air was arriving from aloft and over Canada; and (*e*) Cheeka Peak impactor samples 5, 6, and 7 during westerly airflow. Vertical bars represent the standard deviation of the average distribution.

0.16 and 0.5 μm during RITS 91 and between 0.25 and 0.5 μm both on the ship and at Cheeka Peak during PSI 91.

The lack of NH_4^+ in the smallest size range suggests that it was not involved in new particle production. At larger sizes, NH_3 condensed onto acidic accumulation mode particles but not onto basic, coarse mode sea-salt particles. As it condensed onto accumulation mode particles, the *p*H of those particles should have increased allowing for the condensation of more gas phase acidic H_2SO_4 and MSA. The importance of NH_3 in new particle production cannot be entirely discounted on the basis of these results, however. It may be that because the mass in the smallest particle size range is so low, any NH_4^+ that was present was below the detection limit of 0.006 nmoles m^{-3}.

4.2.2. *Effective surface area size distributions.* The most complete measurement of the number size distribution, 0.02- to 9.6-μm particle diameter, was made during PSI 91 at Cheeka Peak. Since surface area size distributions were derived from number size distributions, they were calculated only for these data. The available particulate surface area size distribution was calculated directly from the number size distribution using

$$dS/d \log D_p = 4\pi r^2 dN/d \log D_p \quad (1)$$

In considering the condensation of a gaseous species onto the surface of a particle, the physical process of the collision of the gas molecule with the particle as a function of particle size also must be taken into account. Hence an effective surface area, S_{eff}, was calculated using

$$S_{eff}(r) = S(r)/(1 + 2r/\pi\lambda) \quad (2)$$

where r is the particle radius and λ is the mean free path of the condensing gas [*Warneck*, 1988]. If the particle radius is such that $2r/\pi\lambda$ is much less than 1, molecules will collide with particles at gas-kinetic rates. For larger particles where $2r/\pi\lambda$ is greater than 1, the collision rate is diffusion controlled and increases with r and not r^2. As a result, S_{eff} is much lower than S for particles with diameters greater than about 0.3 μm. In the following discussion, S_{eff} and not S will be considered.

Cheeka Peak effective surface area size distributions are shown in Figure 6. For samples collected as air was coming from aloft and over Canada, the average sum of S_{eff} over all particle sizes was 34 ± 18 μm^2 cm^{-3} with 5% occurring in the supermicron fraction. For samples collected during onshore flow, the average sum of S_{eff} over all particle diameters was 22 ± 12 μm^2 cm^{-3} with 30% present in the coarse fraction. The maximum in the distribution occurred between 0.3- and 0.5-μm particle diameter.

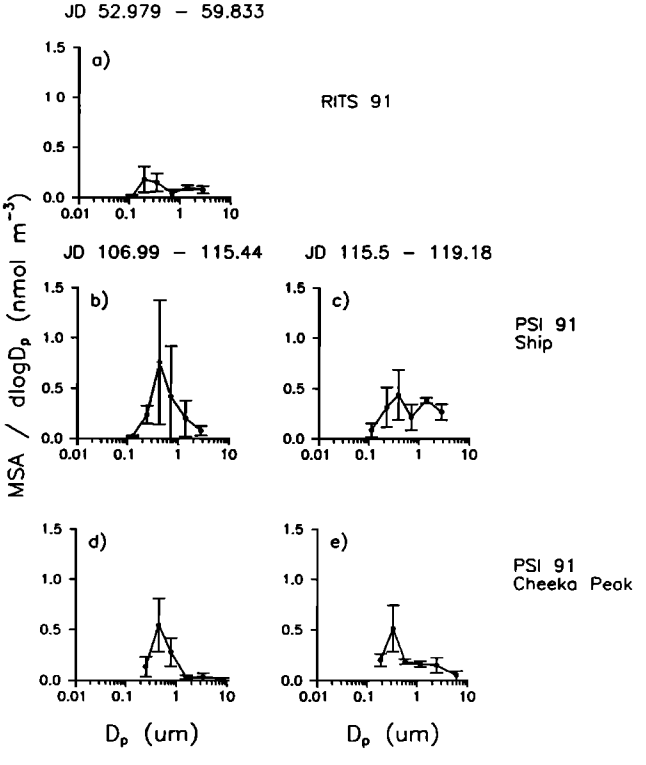

Fig. 4. Mass size distributions of methanesulfonate (MSA) from measurements during RITS 91 and shipboard and Cheeka Peak measurements during PSI 91. Cheeka Peak distributions were based on measurements of dried air and were corrected for relative humidity effects on particle diameters. Average distribution of (*a*) impactor samples 1, 2, 3, 4, and 5 during RITS 91; (*b*) shipboard impactor samples 1, 2, 3, 4, and 5 as air was arriving from aloft and over Canada; (*c*) shipboard impactor samples 6, 7, and 8 during westerly airflow; (*d*) Cheeka Peak impactor samples 1, 2, 3, and 4 as air was arriving from aloft and over Canada; and (*e*) Cheeka Peak impactor samples 5, 6, and 7 during westerly airflow. Vertical bars represent the standard deviation of the average distribution.

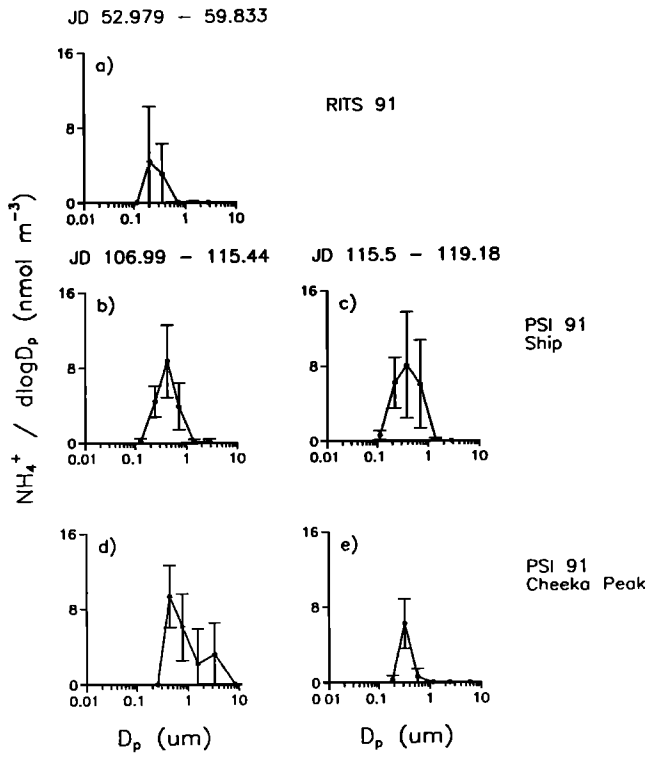

Fig. 5. Mass size distributions of NH_4^+ from measurements during RITS 91 and shipboard and Cheeka Peak measurements during PSI 91. Cheeka Peak distributions were based on measurements of dried air and were corrected for relative humidity effects on particle diameters. Average distribution of (*a*) impactor samples 1, 2, 3, 4, and 5 during RITS 91; (*b*) shipboard impactor samples 1, 2, 3, 4, and 5 as air was arriving from aloft and over Canada; (*c*) shipboard impactor samples 6, 7, and 8 during westerly airflow; (*d*) Cheeka Peak impactor samples 1, 2, 3, and 4 as air was arriving from aloft and over Canada; and (*e*) Cheeka Peak impactor samples 5, 6, and 7 during westerly airflow. Vertical bars represent the standard deviation of the average distribution.

4.2.3. *Relationships between mass and effective surface area size distributions.* The mass and effective surface area size distributions were compared to investigate the role of H_2SO_4, MSA, and NH_3 in new particle production versus particle growth. A corresponding increase in mass and effective surface area within the smallest particle size range would suggest that gas phase precursors were undergoing homogeneous nucleation and subsequent condensational growth to form new particles and particulate mass. Alternatively, a corresponding increase in both mass and effective surface area within all larger size ranges would indicate that gas phase species were condensing onto existing particles and contibuting to particle growth. S_{eff} was summed over the particle size range collected on each impactor stage. Then nss $SO_4^=$, MSA, and NH_4^+ mass were plotted against S_{eff} for all samples collected at Cheeka Peak as a function of impactor stage.

The results for nss $SO_4^=$ are shown in Figure 7. The most statistically significant correlations (meaning those with the highest correlation coefficient and lowest residual values) were found for stages 2 (0.16 to 0.25 μm) and 3 (0.25 to 0.5 μm) where $r^2 = 0.531$ and 0.686, respectively. A trend of increasing S_{eff} with increasing nss $SO_4^=$ mass also was found for stages 5 (1.0 to 2.0 μm) and 6 (2.0 to 4.0 μm) where r^2 equaled 0.653 and 0.679, respectively, but these high values were controlled by two samples that have large values of mass and S_{eff}. With these outliers removed, the correlation becomes much weaker. The corresponding high values of mass and S_{eff} in the largest particle diameters may be a result of the condensation of acidic SO_2 as well as H_2SO_4 onto basic sea-salt particles.

The results of the comparison of MSA mass and S_{eff} are shown in Figure 8. The most statistically significant correlations (highest correlation coefficient and lowest residual values) were found in stages 2 (0.16 to 0.25 μm) and 3 (0.25 to 0.5 μm) with $r^2 = 0.484$ and 0.736, respectively. Stages 4 (0.5 to 1.0 μm), 5 (1.0 to 2.0 μm), and 6 (2.0 to 4.0 μm) also showed a trend of increasing S_{eff} with increasing mass. The correlation coefficients for these stages were similar to those for stages 2 and 3, but the residual values were larger due to the existence of one or two outlying points.

For both nss $SO_4^=$ and MSA, no correlation was found in the smallest size range, but a trend of increasing S_{eff} with increasing mass was found in all larger size ranges. This indicates that most of the nss $SO_4^=$ and MSA was not involved in new particle production but was condensed onto existing aerosol having diameters greater than 0.16 μm.

A correlation was found between NH_4^+ mass and S_{eff} for particles between 0.16 and 0.25 μm ($r^2 = 0.556$) and for particles between 0.25 and 0.5 μm ($r^2 = 0.747$) (Figure 9). The lack of a correlation for both the smallest and the largest particle sizes was dramatic. This supports the conclusion that gas phase NH_3 was not involved in new particle production but instead was condensed onto acidic accumulation mode particles. Again, because of the low mass quantities in the smallest size range it also may be that NH_4^+ was present in the smallest particles but not in detectable amounts. A method which allows for chemical speciation on modest amounts of aerosol mass is needed to clarify further the role of NH_3 in new particle production.

Models [*Warren and Seinfeld*, 1985] and field experiments [*Covert et al.*, 1992] have shown that existing aerosol particles act as a sink for condensing gas phase species and serve to quench new particle production. This was the case during most of PSI 91 when the available particle surface area was more than 5 $\mu m^2\ cm^{-3}$. However, *Covert et al.* [1992] found evidence for new particle production 3 times during the experiment. In one 7-hour period the total particle number concentration between 0.003- and 0.015-μm diameter increased

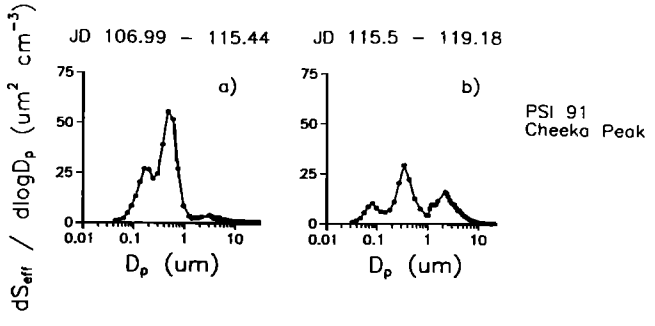

Fig. 6. Particle effective surface area size distributions from Cheeka Peak measurements during PSI 91. S_{eff} was calculated from the number size distribution measured over a range of particle diameters of 0.02 to 9.6 μm. The S_{eff} distributions were corrected for relative humidity effects on particle diameters. Average distribution corresponding to (*a*) Cheeka Peak impactor samples 1, 2, 3, and 4 as air was arriving from aloft and over Canada; and (*b*) Cheeka Peak impactor samples 5, 6, and 7 during westerly airflow.

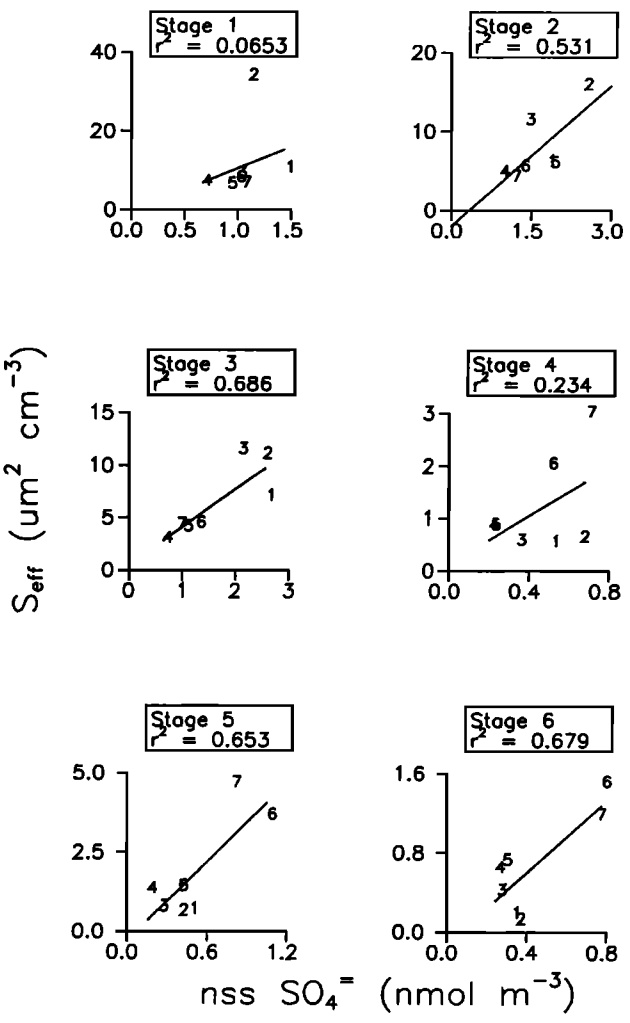

Fig. 7. Non-sea-salt $SO_4^=$ mass versus S_{eff} for samples taken at Cheeka Peak during PSI 91 according to impactor stage. The upper cut size of each stage is 0.16 μm (stage 1), 0.25 μm (stage 2), 0.5 μm (stage 3), 1.0 μm (stage 4), 2.0 μm (stage 5), and 4.0 μm (stage 6). Number labels represent impactor sample.

from about 100 to 3000 cm^{-3}. This increase was associated with a decrease in total available surface area, $S = 4\pi r^2 N$, from 25 to 5 μm^2 cm^{-3}. The long impactor sampling times of 12 to 24 hours prevented the confirmation of this episode of new particle production in the collected samples. The total available surface area averaged over all impactor sampling periods on the ship and at Cheeka Peak was 46 ± 12 and 128 ± 56 μm^2 cm^{-3}. These large values indicate that at least on the time scale over which the mass size distributions were measured, the existing aerosol was acting as a sink for gas phase H_2SO_4, MSA, and NH_3 preventing their nucleation into new particles. However, new particle production could have been happening on shorter time scales.

4.3. *Comparison of Mass and Number Size Distributions*

Mass and number concentration as a function of size were compared to determine if periods of low (high) mass concentration corresponded to periods of low (high) number concentration in a particular size interval. For example, a correspondence between high mass and number concentration in the larger accumulation mode size range would occur if a past increase in the source strength of gas phase H_2SO_4 resulted in the growth of smaller particles to larger diameters.

The effect of an increase in the source strength of a condensing species on the number concentration for a size range corresponding to an impactor stage depends on the shape of the number size distribution within as well as below that size range. As shown in Figure 10*a*, if an increase in mass results in a shift in the maximum of the number size distribution to a larger diameter within the same size range and the slope remains constant, no increase in number will be detected. If the slope is negative and the maximum shifts to the next largest size range, then an increase in number will be detected in the larger size range (see Figure 10*b*). As a result, it is necessary to know where the maximum in the accumulation mode occurs and what the sense of the slope is within each impactor stage. The data analysis therefore involved using the shape of the measured number size distribution to interpret the lack or presence of a corresponding increase in mass and in number within an impactor size interval.

To explore the relationships between mass and number concentrations, number concentrations measured during PSI 91

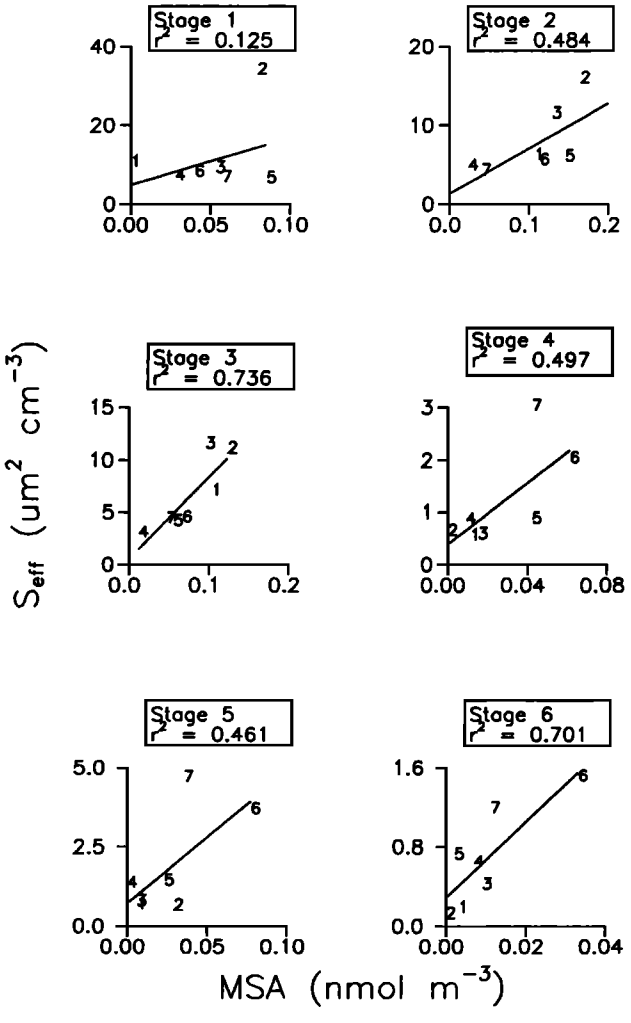

Fig. 8. MSA mass versus S_{eff} for samples taken at Cheeka Peak during PSI 91 according to impactor stage. The upper cut size of each stage is 0.16 μm (stage 1), 0.25 μm (stage 2), 0.5 μm (stage 3), 1.0 μm (stage 4), 2.0 μm (stage 5), and 4.0 μm (stage 6). Number labels represent impactor sample.

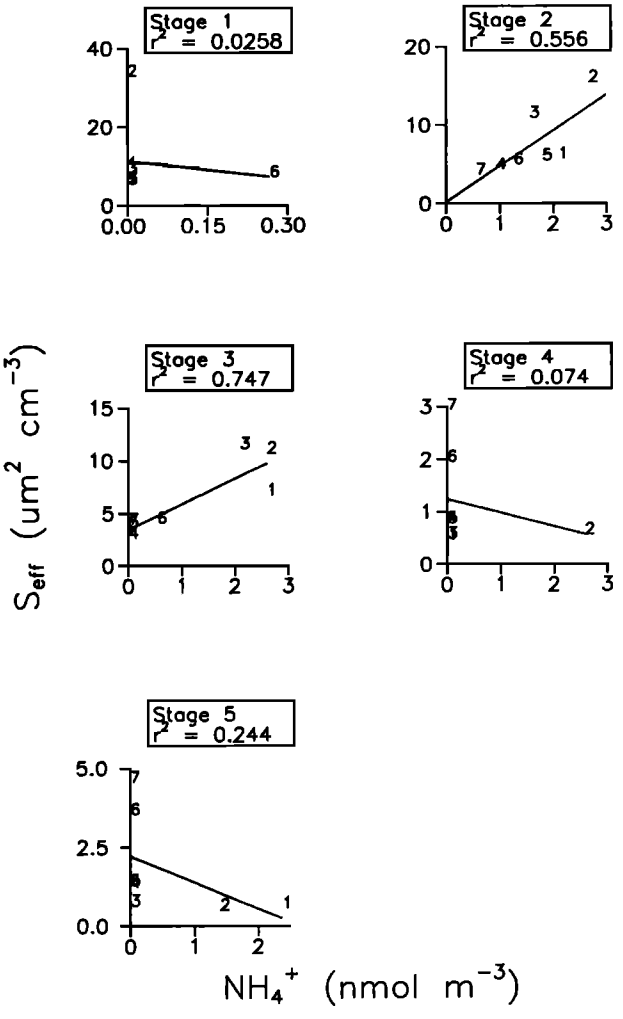

Fig. 9. NH_4^+ mass versus S_{eff} for samples taken at Cheeka Peak during PSI 91 according to impactor stage. The upper cut size of each stage is 0.16 μm (stage 1), 0.25 μm (stage 2), 0.5 μm (stage 3), 1.0 μm (stage 4), 2.0 μm (stage 5), and 4.0 μm (stage 6). Number labels represent impactor sample.

were summed over the particle size range collected on each impactor stage. Then the nss $SO_4^=$, MSA, and NH_4^+ mass were plotted against N for all samples collected on the ship and at Cheeka Peak. The results for the first three impactor stages (0.02 to 0.16 μm, 0.16 to 0.25 μm, and 0.25 to 0.5 μm) are shown in Figures 11, 12, and 13 for nss $SO_4^=$, MSA, and NH_4^+, respectively. Within the smallest size range, 0.02 to 0.16 μm, no correlations were found between number and nss $SO_4^=$, MSA, or NH_4^+ mass in either the shipboard or Cheeka Peak samples. The number concentration varied widely, but the mass concentration remained fairly constant. Only a small percent of the total mass is found in this size range which is to be expected considering the width of the interval and variability of the size distribution.

No correlations were found in the smallest accumulation mode size range (0.16 to 0.25 μm) in the shipboard samples. The mass concentration of all three species varied by up to a factor of 5, but the variation was not reflected by a corresponding change in the number concentration. A change in the number concentration resulted in a shift of the nuclei mode maximum toward a larger diameter within the same impactor stage. As a result, changes in the number concentration were not detected (see Figure 10*a*). A positive correlation was found in the shipboard samples for nss $SO_4^=$, MSA, and NH_4^+ versus number in the largest accumulation mode size range (0.25 to 0.5 μm). Apparently, the condensation of mass onto small accumulation mode particles allowed for their growth to larger diameters. A change in number concentration was detectable because of the negative slope of the number size distribution and the shift of the accumulation mode maximum further into the size range corresponding to the third impactor stage (see Figure 10*b*).

For the shipboard samples a doubling of the nss $SO_4^=$ mass in the 0.25- to 0.5-μm size range corresponded to a 50% increase in number concentration, likewise for a doubling of the NH_4^+ mass. The similarity of the sensitivity of number to nss $SO_4^=$ and NH_4^+ mass may be a result of the acid-base interaction of the two species within the particle. As gas phase NH_3 is absorbed onto the particle, the *p*H increases and the surface acid vapor pressure decreases. This decrease in acid vapor pressure should enhance the condensation of H_2SO_4 onto the particle [*Hoppel et al.*, 1987; *Quinn et al.*, 1992]. A doubling of the MSA mass corresponded to a 30% increase in number concentration.

Unlike the ship data, positive correlations were found for the Cheeka Peak samples between nss $SO_4^=$, MSA, and NH_4^+ mass and number in both the smaller (0.16 to 0.25 μm) and the larger (0.25 to 0.5 μm) accumulation mode size ranges. Differences in the number size distribution at the two sites offer one explanation for this. The higher average relative humidity at Cheeka Peak shifted the number size distribution to larger diameters. In addition, the number concentration of the nuclei mode was larger at Cheeka Peak, resulting in a shift

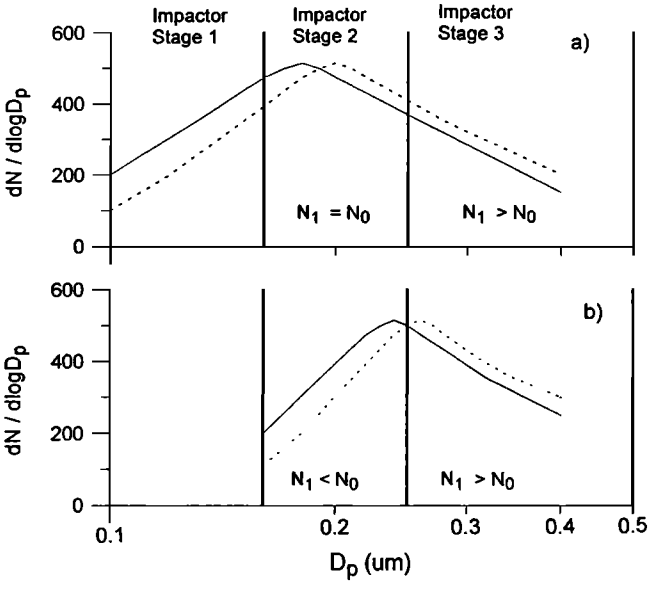

Fig. 10. Effect of the shape of the number size distribution on the change in number concentration within an impactor size interval as the maximum in the size distribution shifts to larger diameters. Impactor stages 1, 2, and 3 correspond to the size intervals <0.16 μm, 0.16 to 0.25 μm, and 0.25 to 0.5 μm, respectively. The solid curve is the initial size distribution and the dashed curve is the distribution after the shift to larger diameters. (*a*) As the size distribution shifts to larger diameters, the slope remains constant and no significant increase in number will be detected ($N_1 = N_0$). (*b*) The maximum shifts into the next impactor size interval such that an increase in number in the larger size interval will be detected ($N_1 > N_0$).

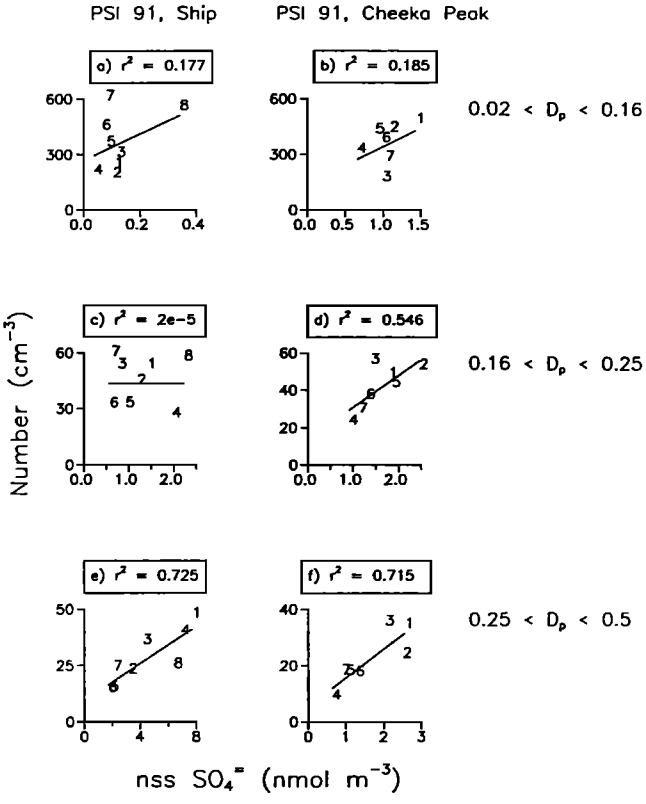

Fig. 11. Non-sea-salt $SO_4^=$ mass versus number concentration for (*a*) shipboard impactor stages corresponding to particle diameters between 0.02 to 0.16 μm, (*b*) Cheeka Peak impactor stages corresponding to particle diameters between 0.02 to 0.16 μm, (*c*) shipboard impactor stages corresponding to particle diameters between 0.16 and 0.25 μm, (*d*) Cheeka Peak impactor stages corresponding to particle diameters between 0.16 and 0.25 μm, (*e*) shipboard impactor stages corresponding to particle diameters between 0.25 and 0.5 μm, and (*f*) Cheeka Peak impactor stages corresponding to particle diameters between 0.25 to 0.5 μm. Number labels represent impactor sample number.

in the minimum between the nuclei and the accumulation mode to a larger diameter. As a result, the right hand slope of the nuclei mode occurred in the size range of the second impactor stage (Figure 10*b*).

For the Cheeka Peak samples a doubling of nss $SO_4^=$ mass corresponded to 50 and 70% increases in the number concentration for impactor stages 2 and 3, respectively. A doubling of the NH_4^+ mass was associated with 40 and 30% increases in number in stages 2 and 3, respectively, and a doubling of the MSA mass corresponded to increases of 50 and 60% in these stages.

Positive correlations also were found in the Cheeka Peak data between nss $SO_4^=$ and MSA mass and number in the largest size ranges of 1.0 to 2.0 and 2.0 to 4.0 μm. However, these correlations were driven by one or two samples which had correspondingly high mass and number concentrations. No correlation was found for NH_4^+ mass and number in these supermicron size ranges.

The results from the comparison between mass and number are similar to those from the comparison between mass and effective surface area. There was no corresponding increase in mass and number in the smallest measured impactor size interval suggesting that H_2SO_4, MSA, and NH_3 were not involved in new particle production. It could be that these gas phase precursors were involved in new particle production on a shorter time scale than that of the 12- to 24-hour impactor sampling period. To chemically detect new particle production on shorter time scales, a more sensitive method of mass analysis is needed. Both H_2SO_4 and MSA appeared to condense onto existing aerosol particles, while NH_3 condensed onto existing accumulation mode particles but not onto coarse mode particles.

4.4. *Comparison of Mass and CCN Number Concentration*

Whether a given particle undergoes activation and becomes a cloud droplet depends on its size, its degree of water solubility, and the ambient supersaturation. *Bigg* [1986] compared CCN concentrations measured over a 4-year period at Cape Grim with those predicted from the CN size distribution assuming a composition of pure NaCl and pure $(NH_4)_2SO_4$. He found that only 40 to 80% of the CN number population were active CCN at 0.3 to 1% supersaturation. Apparently, a particle surface coating of organic material on soluble particles suppressed cloud droplet nucleation. It could also be that a portion of the particle population was composed primarily of compounds less soluble than sulfate and methanesulfonate salts. Because of changing local conditions such as relative humidity, degree of cloud cover, rainfall rate,

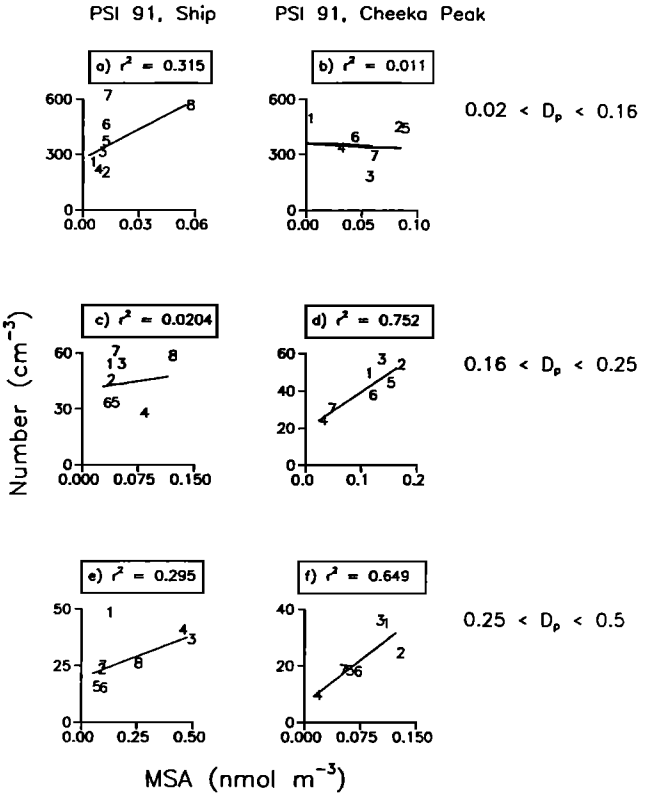

Fig. 12. MSA mass versus number concentration for (*a*) shipboard impactor stages corresponding to particle diameters between 0.02 to 0.16 μm, (*b*) Cheeka Peak impactor stages corresponding to particle diameters between 0.02 to 0.16 μm, (*c*) shipboard impactor stages corresponding to particle diameters between 0.16 and 0.25 μm, (*d*) Cheeka Peak impactor stages corresponding to particle diameters between 0.16 and 0.25 μm, (*e*) shipboard impactor stages corresponding to particle diameters between 0.25 and 0.5 μm, and (*f*) Cheeka Peak impactor stages corresponding to particle diameters between 0.25 to 0.5 μm. Number labels represent impactor sample number.

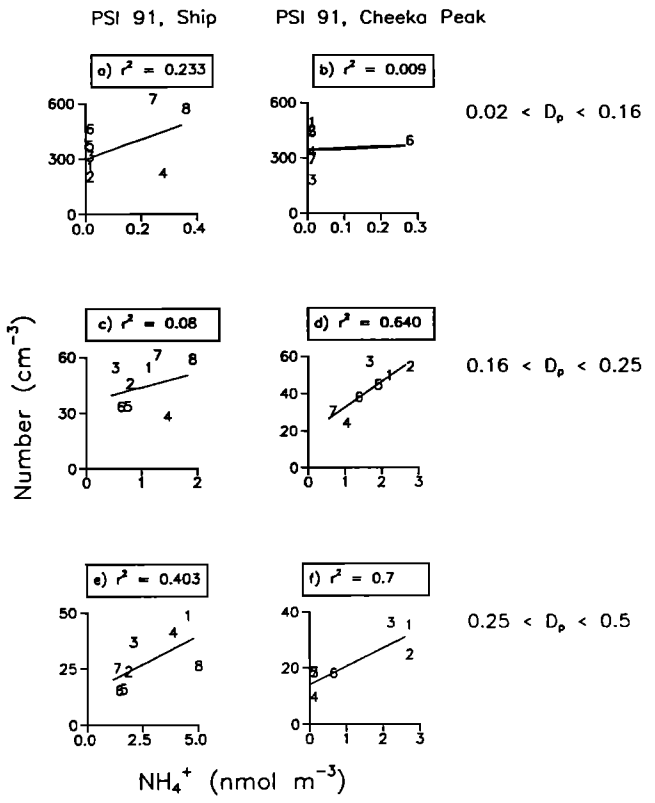

Fig. 13. NH_4^+ mass versus number concentration for (*a*) shipboard impactor stages corresponding to particle diameters between 0.02 to 0.16 μm, (*b*) Cheeka Peak impactor stages corresponding to particle diameters between 0.02 to 0.16 μm, (*c*) shipboard impactor stages corresponding to particle diameters between 0.16 and 0.25 μm, (*d*) Cheeka Peak impactor stages corresponding to particle diameters between 0.16 and 0.25 μm, (*e*) shipboard impactor stages corresponding to particle diameters between 0.25 and 0.5 μm, and (*f*) Cheeka Peak impactor stages corresponding to particle diameters between 0.25 to 0.5 μm. Number labels represent impactor sample number.

and wind speed, the number of CN which will grow to CCN size and activate before removal from the atmosphere is variable and difficult to predict. As a result, one of the largest uncertainties in the DMS/CCN/climate system is the sensitivity of the CCN number population to changes in particulate mass concentrations.

There are many source and sink processes controlling the burden of particulate mass which will affect the relationship between mass and CCN number concentrations. If source and sink processes influence the burdens of mass and CCN similarly, a correlation between the two should be detectable. For example, this would be the case if fresh mass were associated with particle production, these new particles grew into the accumulation mode size range so that they were large enough to activate at the ambient supersaturation before being removed from the atmosphere, and the time scale of removal of CN by deposition processes was longer than the time scale of activation.

CCN concentrations at 0.3% supersaturation were measured during PSI 91 at Cheeka Peak. At this supersaturation all particles with diameters greater than 0.073 μm should activate assuming a composition of pure $(NH_4)_2SO_4$ [*Fletcher*, 1962]. CCN concentrations were averaged over the period of each impactor sample so that they could be compared to nss $SO_4^=$ and MSA mass concentrations. The total mass concentration summed over all impactor stages was used in the comparison. Only four out of seven impactor samples were used as CCN concentrations measured during the sampling periods of the remaining three were not meaningful because of the presence of fog. As a result, conclusions made about the relationship between CCN number concentration and mass concentration are limited because of the small sample number. However, these data can be put into a broader context by comparing them to previously reported data sets.

During this experiment a doubling of the nss $SO_4^=$ mass corresponded to a 40% increase in the CCN number concentration (Figure 14). The existence of a nonzero y intercept could be a result of a particle composition that is less soluble than pure $(NH_4)_2SO_4$. A comparison of the CCN concentration and the total particle concentration greater than 0.073 μm reveals that only 48 ± 13% of the particles were activated at 0.3% supersaturation. Less soluble particles would require larger diameters for activation to occur at 0.3% supersaturation. These data suggest that only when the particle diameter and fraction of soluble mass are sufficient does a relationship exist between nss $SO_4^=$ mass and CCN concentration.

No statistically significant correlation was found between the MSA mass and the CCN number concentration (Figure 14). It may be that correlations between MSA and CCN concentration are detectable only when MSA has a sizeable contribution to

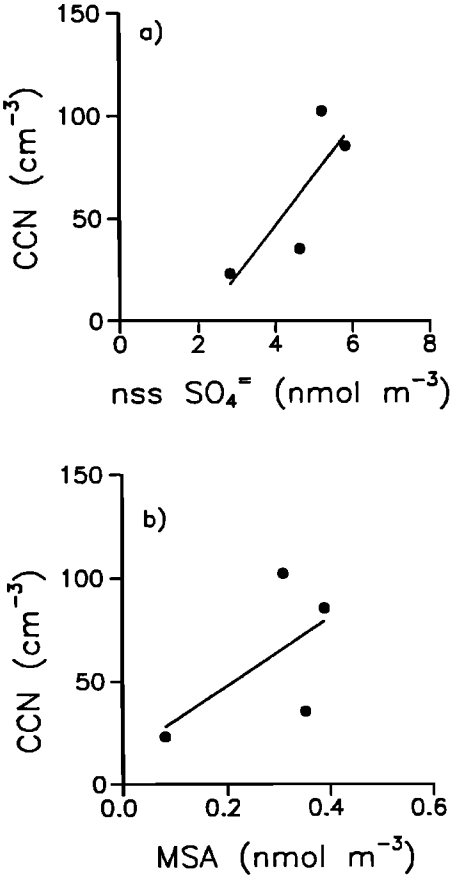

Fig. 14. Comparison for four PSI 91 Cheeka Peak impactor samples of (*a*) the summed nss $SO_4^=$ concentration over all impactor stages versus CCN concentration at 0.3% supersaturation and (*b*) the summed MSA concentration over all impactor stages versus CCN concentration at 0.3% supersaturation.

the total particulate soluble mass. When it is a small fraction, as it was here, its effect on the CCN concentration may be too slight to observe.

Other recently reported results have indicated that a relationship exists between nss $SO_4^=$ and MSA mass and CCN number concentrations. During PSI 89 and 90 off the coast of Washington State, *Hegg et al.* [1991] made measurements aloft of nss $SO_4^=$ particulate mass and CCN number concentrations at 1% supersaturation. A doubling of the mass concentration from 2 to 4 nmol m^{-3} corresponded to a 40% increase in CCN concentration. *Ayers and Gras* [1991] found a correlation between MSA mass and CCN number concentration in a 9-year data record of measurements made at Cape Grim. The relationship is linear at low concentrations of MSA but flattens at high concentrations. The authors suggest that once a certain amount of particulate surface area is available, additional gas phase mass condenses onto the existing particles instead of forming new particles. The linear portion of the correlation is such that a doubling of MSA mass corresponds to a 30% increase in CCN number concentration at 0.23% supersaturation and a 40% increase at 1.2% supersaturation. The positive intercept indicates that there is a significant number of particles which were activated to become CCN that contained negligible amounts of MSA.

Both the Northeast Pacific and Cape Grim measurements indicate that a doubling of the DMS-derived particulate mass corresponds to about a 30 to 40% increase in the CCN number concentration. This consistency exists even though the percent supersaturation of the CCN measurements and, hence, the critical diameter for activation varied. This suggests that larger diameter particles, i.e., those that activate below 1.2% supersaturation, have the greatest effect on the CCN number concentration. As the measured number concentration of small particles is not negligible, it must be their chemical composition that limits their effect on the CCN number concentration.

Clearly, evidence exists for a relationship between nss $SO_4^=$ and MSA mass and CCN number concentration. Because of the number of processes which control the formation and removal of mass and CCN in the atmosphere, the relationship is complex and varies with local conditions. Simultaneous measurement of chemical mass size distributions, number size distributions, CCN number concentrations, and meteorological parameters at a variety of locations are needed to further characterize and quantify the relationship.

5. CONCLUSIONS

In an attempt to quantify particulate mass and number relationships within the DMS/CCN/climate system, simultaneous measurements of nss $SO_4^=$, MSA, and NH_4^+ mass size distributions, particle number size distributions, and CCN number concentrations were made over the northeastern Pacific Ocean in April and May 1991. In addition, measurements of the mass size distribution of nss $SO_4^=$, MSA, and NH_4^+ were made over the central Pacific Ocean during February 1991. The nss $SO_4^=$ and MSA size distributions were bimodal with significant mass in both the submicron and the supermicron size fractions. The supermicron nss $SO_4^=$ could have been a result of condensation of gaseous SO_2 onto basic sea-salt particles. Open ocean measurements of the MSA size distribution revealed more MSA in the supermicron fraction than was found in the coastal measurements. This is in agreement with previously reported data [*Pszenny*, 1992; *Huebert et al.*, 1993] and may reflect relatively higher coarse mode and/or lower fine mode number concentrations in open ocean regions. No NH_4^+ was detected in the smallest measured size range and very little was found in the largest particles. Instead, it was concentrated in larger accumulation mode acidic particles (0.25- to 0.5-μm diameter).

Based on measurements over the northeastern Pacific Ocean, particulate nss $SO_4^=$, MSA, and NH_4^+ mass appeared to be correlated with both particle effective surface area and number in the accumulation mode size range (0.16 to 0.5 μm). No correlations were found in the smallest measured size range (<0.16 μm). Apparently, on the 12- to 24-hour time scale of these measurements, H_2SO_4, MSA, and NH_3 did not contribute significantly to new particle production but instead allowed for the growth of small accumulation mode particles to larger diameters. The sensitivity of number to mass was such that a doubling of nss $SO_4^=$, MSA, and NH_4^+ mass corresponded to about a 50, 40, and 45% increase in number in the accumulation mode size range, respectively.

A correlation also was found between nss $SO_4^=$ mass and CCN number concentration such that a doubling of the mass corresponded to a 40% increase in the number concentration. No correlation was found between MSA mass and CCN concentration, however. MSA made up a very small percent of the total soluble particulate mass which may have made a correlation difficult to detect.

Based on these results, there appear to be quantifiable relationships between particulate mass and both CN and CCN number concentration. However, these relationships are complex due to the number of controlling processes involved and their varying time scales. In addition, the relationships will vary with local conditions, including meteorological parameters, the DMS source strength, and atmospheric oxidant levels. The ultimate goal of measurements such as those made here is to quantify the DMS/CCN/climate system under a variety of local physical and chemical conditions and to use the results as input into global chemical climate models. Therefore the in situ measurement techniques used will have to perform with adequate sensitivity on the time scale of mixing within the marine boundary layer (≅ an hour).

These requirements apply to both gas and particle phase chemical measurements. As shown here, the simultaneous measurement of mass and number size distributions is useful in studying how the DMS oxidation products are distributed between particle production and growth. However, existing methods for measuring mass size distributions need to be modified or new techniques developed such that these size distributions can be measured on a shorter time scale and with a greater sensitivity.

Acknowledgments. We thank J. Benson for analytical assistance, R. Artz for air mass trajectory analysis, R. Charlson for helpful discussions, and the officers and crew of the NOAA ship *Discoverer* for their help and cooperation. This work was funded in part by the NOAA Climate and Global Change Program and the NASA Interdisciplinary Studies Program. This is JISAO contribution 229 and NOAA PMEL contribution number 1392.

REFERENCES

Albrecht, B. A., Aerosols, cloud microphysics, and fractional cloudiness, *Science, 245*, 1227–1230, 1989.

Andreae, M. O., H. Berresheim, T. W. Andreae, M. A. Kritz, T. S. Bates, and J. T. Merrill, Vertical distribution of dimethylsulfide, sulfur dioxide, aerosol ions, and radon over the Northeast Pacific Ocean, *J. Atmos. Chem., 6*, 149–173, 1988.

Ayers, G. P., and J. L. Gras, Seasonal relationship between cloud

condensation nuclei and aerosol methanesulfonate in marine air, *Nature, 353*, 834–835, 1991.
Baron, P. A., Calibration and use of the aerodynamic particle sizer (APS 3300), *Aerosol Sci. Technol., 5*, 55–67, 1986.
Bates, T. S., R. J. Charlson, and R. H. Gammon, Evidence for the climatic role of marine biogenic sulfur, *Nature, 329*, 319–320, 1987.
Bates, T. S., J. A. Calhoun, and P. K. Quinn, Variations in the methanesulfonate to sulfate molar ratio in submicrometer marine aerosol particles over the South Pacific Ocean, *J. Geophys. Res., 97*, 9859–9865, 1992.
Berner, A., C. Lurzer, F. Pohl, O. Preining, and P. Wagner, The size distribution of the urban aerosol in Vienna, *Sci. Total Environ., 13*, 245–261, 1979.
Berresheim, H., Biogenic sulfur emissions from the Subantarctic and Antarctic oceans, *J. Geophys. Res., 92*, 13,245–13,262, 1987.
Berresheim, H., M. O. Andreae, G. P. Ayers, R. W. Gillett, J. T. Merrill, V. J. Davis, and W. L. Chameides, Airborne measurements of dimethylsulfide, sulfur dioxide, and aerosol ions over the southern ocean south of Australia, *J. Atmos. Chem., 10*, 341–370, 1990.
Bigg, E. K., Discrepancy between observation and prediction of CCN concentrations, *Atmos. Res., 20*, 82–86, 1986.
Bigg, E. K., J. L. Gras, and C. Evans, Origin of Aitken particles in remote regions of the southern hemisphere, *J. Atmos. Chem., 1*, 203–214, 1984.
Calhoun, J. A., T. S. Bates, and R. J. Charlson, Sulfur isotope measurements of submicrometer aerosol particles over the Pacific Ocean, *Geophys. Res. Lett., 18*, 1877–1880, 1991.
Cantoni, G., and D. G. Anderson, Enzymatic cleavage of dimethyl propiothetin by Polysiphonia larosa, *J. Biol. Chem., 222*, 171–177, 1956.
Charlson, R. J., D. S. Covert, T. V. Larson, and A. P. Waggoner, Chemical properties of tropospheric sulfur aerosols, *Atmos. Environ., 12*, 39–53, 1978.
Charlson, R. J., J. E. Lovelock, M. O. Andreae, and S. G. Warren, Oceanic phytoplankton, atmospheric sulfur, cloud albedo and climate, *Nature, 326*, 655–661, 1987.
Coakley, J. A., R. L. Bernstein, and P. A. Durkee, Effect of ship-stack effluents on cloud reflectivity, *Science, 237*, 1020–1022, 1987.
Covert, D. S., V. N. Kapustin, P. K. Quinn, and T. S. Bates, New particle formation in the marine boundary layer, *J. Geophys. Res., 97*, 20,581–20,589, 1992.
Dacey, J. W. H., and N. V. Blough, Hydroxide decomposition of dimethylsulfoniopropionate to form dimethylsulfide, *Geophys. Res. Lett., 14*, 1246–1249, 1987.
Draxler, R. R., Hybrid single-particle Lagrangian integrated trajectories (HY-SPLIT): Version 3.0—User's guide and model description, *NOAA Tech. Rep., ERL ARL-195*, 1992.
Durkee, P. A., F. Pfeil, E. Frost, and R. Shema, Global analysis of aerosol particle characteristics, *Atmos. Environ., 25*, 2457–2471, 1991.
Falkowski, P. G., Y. Kim, Z. Kolber, C. Wilson, C. Wrick, and R. Cess, Natural versus anthropogenic factors affecting low-level cloud albedo over the North Atlantic, *Science, 256*, 1311–1313, 1992.
Fletcher, N. H., *The Physics of Rain Clouds*, p. 59, Cambridge University Press, New York, 1962.
Hegg, D. A., L. F. Radke, and P. V. Hobbs, Measurements of Aitken nuclei and cloud condensation nuclei in the marine atmosphere and their relation to the DMS-cloud-climate hypothesis, *J. Geophys. Res., 96*, 18,727–18,733, 1991.
Hegg, D. A., P. Yuen, and T. V. Larson, Modeling the effects of heterogeneous cloud chemistry on the marine particle size distribution, *J. Geophys. Res., 97*, 12,927–12,933, 1992.
Hoppel, W. A., Nucleation in the MSA-water vapor system, *Atmos. Environ., 21*, 2703–2709, 1987.
Hoppel, W. A., J. W. Fitzgerald, G. M. Frick, R. E. Larson, and B. J. Wattle, Preliminary investigation of the role that DMS and cloud cycles play in the formation of the aerosol size distribution, *NRL Rep. 9032*, Nav. Res. Lab., Washington, D. C., 1987.
Huebert, B. J., S. Howell, P. Laj, J. E. Johnson, T. S. Bates, P. K. Quinn, V. Yegorov, A. D. Clarke, and J. N. Porter, Observations of the atmospheric sulfur cycle on SAGA 3, *J. Geophys. Res.*, in press, 1993.
Johnson, J. E., and W. Mitchell, Structure of the marine boundary layer over the Pacific Ocean during the RITS 88 and RITS 89 cruises, *NOAA Data Rep., ERL PMEL-27*, 1991.
Keady, P. B., F. R. Quant, and G. S. Sem, Differential mobility particle sizer: A new instrument for high resolution aerosol size distribution measurements below 1 μm, *TSI Q., 9*, 3–11, 1983.
Kreidenweis, S. M., J. E. Penner, F. Yin, and J. H. Seinfeld, The effects of dimethylsulfide upon marine aerosol concentrations, *Atmos. Environ., 25(A)*, 2501–2511, 1991.
Legrand, M., C. Feniet-Saigne, E. S. Saltzman, C. Germain, N. I. Barkov, and V. N. Petrov, Ice-core record of oceanic emissions of dimethylsulfide during the last climate cycle, *Nature, 350*, 144–146, 1991.
Liu, B. Y. H., and K. W. Lee, Efficiency of membrane and Nuclepore filters for sub-micrometer aerosols, *Environ. Sci. Technol., 10*, 345–350, 1976.
Liu, B. Y. H., and D. Pui, On the performance of the electrical aerosol analyzer, *J. Aerosol Sci., 6*, 249–264, 1975.
Nguyen, B. C., B. Bonsang, and A. Gaudry, The role of the ocean in the global atmospheric sulfur cycle, *J. Geophys. Res., 88*, 10,903–10,914, 1983.
Pszenny, A. A. P., Particle size distributions of methanesulfonate in the tropical Pacific marine boundary layer, *J. Atmos. Chem, 14*, 273–284, 1992.
Pszenny, A. A. P., A. J. Castelle, R. A. Duce, and J. N. Galloway, A study of the sulfur cycle in the Antarctic marine boundary layer, *J. Geophys. Res., 94*, 9818–9830, 1989.
Quinn, P. K., and T. S. Bates, Collection efficiencies of a tandem sampling system for atmospheric aerosol particles and gaseous ammonia and sulfur dioxide, *Environ. Sci. Technol., 23*, 736–739, 1989.
Quinn, P. K., W. E. Asher, and R. J. Charlson, Equilibria of the marine multiphase ammonia system, *J. Atmos. Chem., 14*, 11–30, 1992.
Radke, L. F., J. A. Coakley, Jr., and M. D. King, Direct and remote sensing observations of the effects of ships on clouds, *Science, 246*, 1146–1149, 1989.
Raes, F., and R. Van Dingenen, Simulations of condensation and cloud condensation nuclei from biogenic SO_2 in the remote marine boundary layer, *J. Geophys. Res., 97*, 12,901–12,912, 1992.
Reineking, A., and J. Porstendorfer, Measurements of particle loss functions in a differential mobility analyzer for different flow rates, *Aerosol Sci. Technol., 5*, 483–487, 1986.
Saltzman, E. S., D. L. Savoie, R. G. Zika, and J. M. Prospero, Methane sulfonic acid in the marine atmosphere, *J. Geophys. Res., 88*, 10,897–10,902, 1983.
Saltzman, E. S., D. L. Savoie, J. M. Prospero, and R. G. Zika, Elevated atmospheric sulfur levels off the Peruvian coast, *J. Geophys. Res., 91*, 7913–7918, 1986.
Savoie, D. L., and J. M. Prospero, Particle size distribution of nitrate and sulfate in the marine atmosphere, *Geophys. Res. Lett., 9*, 1207–1210, 1982.
Tang, I. N., H. R. Munkelwitz, and J. G. Davis, Aerosol growth studies, II, Preparation and growth measurements of monodisperse salt aerosols, *J. Aerosol Sci., 8*, 149–159, 1977.
Twomey, S., Pollution and planetary albedo, *Atmos. Environ., 8*, 1251–1256, 1974.
Twomey, S., The influence of pollution on the shortwave albedo of clouds, *J. Atmos. Sci., 34*, 1149–1152, 1977.
Warneck, P., *Chemistry of the Natural Atmosphere, Int. Geophys. Ser.*, vol. 41, 757 pp., Academic, San Diego, Calif., 1988.
Warren, D. R., and J. H. Seinfeld, Prediction of aerosol concentration resulting from a burst of nucleation, *J. Colloid Interface Sci., 105*, 136–142, 1985.
Zang, Z., and B. Y. H. Liu, Performance of TSI 3760 condensation nuclei counter at reduced pressures and flow rates, *Aerosol Sci. Technol., 15*, 228–238, 1991.

T. S. Bates, P. K. Quinn, and D. C. Ramsey-Bell, NOAA/PMEL, 7600 Sand Point Way NE, Seattle, WA 98115.
D. S. Covert, Department of Environmental Health, University of Washington, Seattle, WA 98195.
V. N. Kapustin, Institute of Atmospheric Physics, Russian Academy of Sciences, Moscow, Russia.
L. M. McInnes, Department of Chemistry, University of Washington, Seattle, WA 98195.

(Received October 13, 1992;
revised January 25, 1993;
accepted February 23, 1993.)